



Onset of turbulence in particle-laden pipe flows

Willian Hogendoorn ¹, Bidhan Chandra,^{1,2} and Christian Poelma ^{1,*}

¹*Multiphase Systems (3ME-P&E), Delft University of Technology, Leeghwaterstraat 39,
2628 CB Delft, Netherlands*

²*Chemical Engineering, Indian Institute of Science Education and Research, Bhopal 462066, India*



(Received 3 May 2021; accepted 28 March 2022; published 11 April 2022)

We propose a scaling law for the onset of turbulence in pipe flow of neutrally buoyant suspensions. This scaling law, based on a large set of experimental data, relates the amplitude of the particle-induced perturbations ϵ to the critical suspension Reynolds number $Re_{s,c}$. Here ϵ is a function of the particle-to-pipe diameter ratio and the volume fraction of the suspended particles, $\epsilon = (d/D)^{1/2}\phi^{1/6}$. $Re_{s,c}$ is found to scale as ϵ^{-1} . Furthermore, the perturbation amplitude allows a distinction between classical, intermediate, and particle-induced transitions.

DOI: [10.1103/PhysRevFluids.7.L042301](https://doi.org/10.1103/PhysRevFluids.7.L042301)

The recurrent questions of when and how pipe flow transitions to turbulence long predate the seminal pipe flow experiments by Reynolds in the early 1880s [1]. Since pipe flow is linearly stable, finite-amplitude perturbations are thus responsible for this onset of turbulence [2,3]. For increasing Reynolds number ($Re = UD/\nu$, where U is the bulk velocity, D is the pipe diameter, and ν is the kinematic viscosity), smaller perturbation amplitudes are sufficient to initiate this transition [4]. Initially, turbulence is found to be transient: localized patches of turbulence are embedded in a laminar flow. These turbulent puffs are known to have an increasing lifetime for an increasing Reynolds number [5,6]. Beyond a Reynolds number of 2040, puffs grow and split, eventually leading to sustained turbulence [7].

Particle-laden flows are known to exhibit significantly different transition behavior [8–11]. This is particularly evident from the critical Reynolds number Re_c , which is known to strongly depend on the particle volume fraction ϕ and the particle-to-pipe diameter ratio d/D of the suspended particles. For an increasing volume fraction and a large enough d/D , critical (suspension) Reynolds numbers as low as 600 are reported [8]. Furthermore, beyond a critical volume fraction, which depends on the particle-to-pipe diameter ratio, a different regime is observed: the transition is smooth without the presence of turbulent puffs [9,10]. The exact onset of turbulence is of major importance for a variety of applications, as this onset is accompanied by a significant—sometimes intermittent—drag increase. Precise control over the flow rate (by means of a driving pressure) is essential for process control, whether it is in additive manufacturing, food processing, slurry transport, or dredging. However, despite considerable efforts, a definite scaling indicating the onset of the drag increase in the transitional regime is still absent. We propose a scaling for Re_c in neutrally buoyant suspensions, which is supported by a large set of experimental data.

The first detailed study reporting a prominent effect of particles on laminar-turbulent transition was performed by Matas *et al.* [8]. They determined Re_c for a wide range of d/D and ϕ , using the low-frequency component in the pressure spectrum as an indicator for the presence of turbulent puffs, characteristic of the onset of turbulence. This Re_c was based on the corrected viscosity using

*c.poelma@tudelft.nl

Krieger's viscosity model [12] to account for the presence of particles. A scaling in terms of $\phi D/d$ as a function of this viscosity-corrected critical Reynolds number $\text{Re}_{s,c}$ was proposed to collapse all results on a single master curve. However, the ratio D/d is used in both axes of this master curve, suggesting that $\text{Re}_{s,c}$ is a function of only ϕ .

Lashgari *et al.* [13] studied the influence of neutrally buoyant particles ($d/h = 0.1$, with h being the channel height) numerically for a channel flow configuration. They introduced a distinction based on the dominant term in the stress budget. Three different regimes are identified: a laminar regime for low volume fractions and low Reynolds numbers, a turbulent regime for low volume fractions and high Reynolds numbers, and an inertial shear-thickening regime for $\phi \gtrsim 0.15$. This distinction is feasible only in numerical studies as it requires very detailed flow information.

A different transition mechanism, without the presence of turbulent puffs in the transition region, was found by Hogendoorn and Poelma [9] for higher volume fractions ($\phi \geq 0.175$). This particle-induced transition behavior is characterized by a smooth transition curve, which collapses on $64/\text{Re}$ for low Re_s after viscosity correction. The onset of turbulence was identified using a 10% deviation from the Hagen-Poiseuille law. Agrawal *et al.* [10] independently reported this particle-induced transition for higher volume fractions as well.

This smooth, particle-induced transition was also found for lower volume fractions ($\phi = 0.05$) in combination with a larger particle-to-pipe diameter ratio ($d/D = 0.17$) by Leskovec *et al.* [11]. The authors proposed a scaling to distinguish between classical and particle-induced transitions based on a model of viscous dissipation and particle agitation.

Hogendoorn *et al.* [14] showed that for large d/D even very dilute systems ($\phi = 0.0025$) exhibit this particle-induced transition. Based on instantaneous velocity measurements, they showed that particles introduce perturbations and formulated a model predicting that these disturbances are proportional to d/D and U .

Based on these previous studies, it appears that the onset of turbulence in particle-laden flows is dependent on at least two parameters: the particle-to-pipe diameter ratio and the volume fraction. We propose a scaling for this onset in neutrally buoyant suspensions based on a wide range of experimental data, both our own and from the aforementioned studies. Furthermore, this scaling can be used to predict which transition behavior will be observed for a given system.

Experiments are performed in two different pipe-flow facilities. The first experimental setup is the same as the setup described in Hogendoorn and Poelma [9]. In short, this setup consists of a precision glass pipe with a diameter D of 10.00 ± 0.01 mm. The flow is gravity driven using an overflow reservoir to prevent perturbations from the pumps. The height of this reservoir can be adjusted to control Re_s . At the inlet a settling chamber and a smooth contraction are used to maintain (single-phase) laminar flows for Reynolds numbers exceeding 4000. An orifice, similar to the one used by Wagnowski and Champagne [15], is used to ensure a controlled transition at a fixed Reynolds number of 2000 for single-phase flows. The total pipe length L after the orifice is $310D$. The pressure drop Δp is measured (Validyne DP15) from $125D$ to $250D$, ensuring sufficient development length. Re_s is determined with an uncertainty smaller than 0.5% by collecting and weighing an amount of suspension from the outflow during a given time. A set of peristaltic pumps is used to feed the outflow back to the overflow reservoir.

The second experimental setup is similar to the one described above; for brevity only the differences will be addressed. This setup consists of a polymethyl methacrylate (PMMA) pipe with an inner diameter of 19.98 ± 0.06 mm. Using a settling chamber with a smooth contraction in combination with smooth pipe connectors, a laminar flow is maintained for single-phase Reynolds numbers up to 5000. In this setup the flow is either perturbed using an orifice or perturbed using an active perturbation mechanism, which is a zero-net mass flux injector (adapted from Draad *et al.* [16]) at the beginning of the pipe (positioned $10D$ after the inlet chamber). The perturbation method is no longer significant beyond a certain critical volume fraction, as was reported by Matas *et al.* [8] and Agrawal *et al.* [10]. We also confirmed this for our experiments. The average pressure drop is obtained from $125D$ to $200D$ after this active perturbation. An inline Coriolis mass flow meter (KROHNE Optimax 7050c) is used to measure the flow rate with a maximum uncertainty of

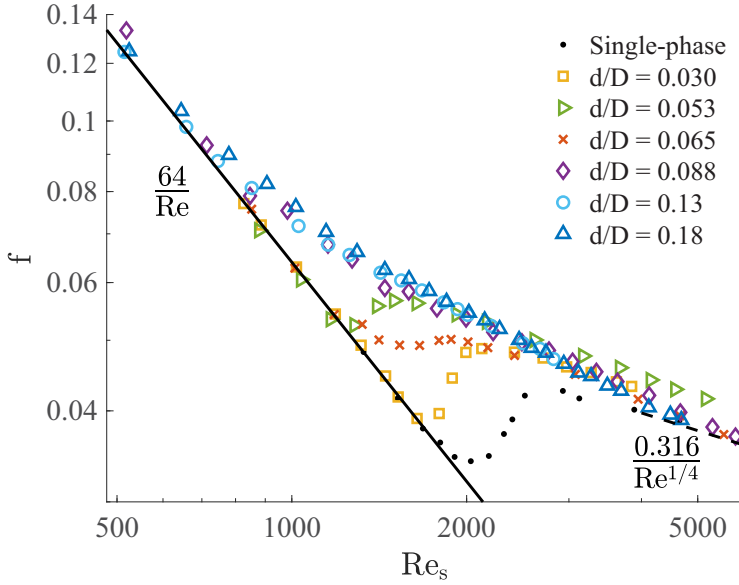


FIG. 1. Friction factor f as a function of the suspension Reynolds number Re_s . The single-phase case is shown for reference. For the particle-laden cases the concentration ϕ is fixed at 0.05 to highlight the diameter-ratio (d/D) effect.

$\pm 0.1\%$. A progressive cavity pump (Monopump, AxFlow B.V.) is used to transport the suspension back to the feeding reservoir. For $d/D = 0.088$, the overflow was removed to be able to drive very viscous flows. We confirmed that this did not influence the (single-phase) transition, as it was still dominated by the orifice perturbation.

Saline water (Na_2SO_4) or a water-glycerin mixture is used to obtain a density-matched system with polystyrene particles (Synthos EPS; density $\rho = 1.032$ kg/L). The volume fraction in the experimental facilities is controlled based on the mass ratio of the working fluid and the particles. Starting with a single-phase system, with a known initial mass, particles are added in steps to obtain the desired volume fraction. Particles with diameters of 0.30 ± 0.034 , 0.53 ± 0.05 , 1.31 ± 0.07 , and 1.75 ± 0.12 mm are used. All four particle types are used in the 10.00 mm facility, and the 1.31 and 1.75 mm particles are also used in the 19.98 mm facility. This results in six d/D ratios (0.03, 0.053, 0.065, 0.088, 0.13, and 0.18); two pressure data sets were reused from previous studies ($d/D = 0.18, 0.053$ [9,14]).

The (critical) Reynolds numbers reported in this study are based on the corrected viscosity ($\mu_s = \rho \nu_s$) of the suspension, determined using Eilers's viscosity model [17]:

$$\frac{\mu_s}{\mu_0} = \left(1 + 1.25 \frac{\phi}{1 - \phi/0.64} \right)^2. \quad (1)$$

Here μ_0 is the viscosity of the continuous phase (i.e., saline water or glycerol).

Figure 1 shows the transition behavior for a range of different experiments (i.e., various d/D) for a constant volume fraction, $\phi = 0.05$. Here the Darcy friction factor [$f \equiv \Delta p / (\frac{1}{2} \rho U^2 L/D)$] is shown as a function of Re_s . The solid line represents the Hagen-Poiseuille law: $64/Re$, the solution for laminar flows. The dashed line shows Blasius's equation. The single-phase case obtained in the 10.00 mm diameter setup, shown for reference, displays a transition at $Re_{s,0} \approx 2000$, resulting from the perturbation in the beginning of the setup. For the particle-laden cases, the influence of d/D is clearly visible from the decrease of $Re_{s,c}$ for increasing d/D . For $d/D < 0.065$, a sharp transition is observed with a clear local minimum in the transition region. This local minimum shifts to lower

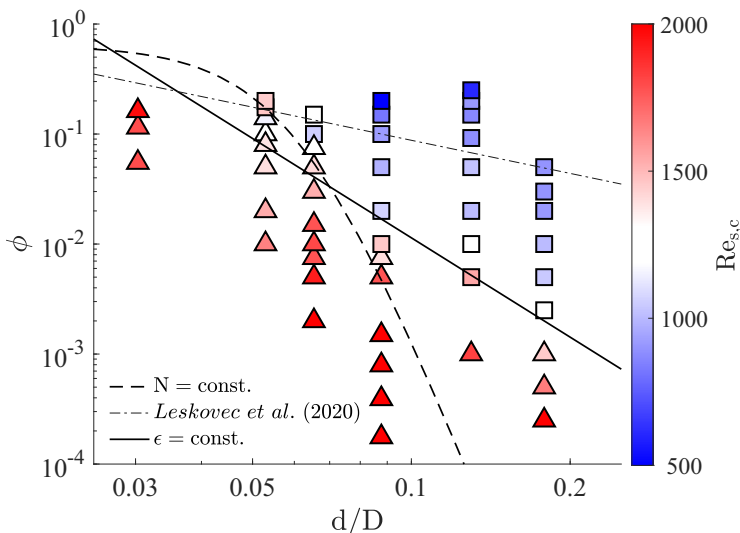


FIG. 2. Regime map ϕ vs d/D , where each marker represents one complete transition curve. The transition curves indicated with the triangles have a local minimum, whereas the transition curves with a monotonically decreasing friction factor are represented by squares. The marker color represents the critical suspension Reynolds number $Re_{s,c}$.

$Re_{s,c}$ for increasing d/D , implying an earlier onset of turbulence. A critical transition curve is shown for $d/D = 0.065$, where the local minimum is still (only just) present. Eventually, for $d/D > 0.065$, smooth transition curves are observed, characteristic of particle-induced transition.

Notably, for the intermediate case ($d/D = 0.065$), the friction factors in the transition region are *lower* compared to the friction factors corresponding to $d/D = 0.053$. Related to this change in transition behavior is the nonmonotonically decreasing critical Reynolds number in this specific region. This can likely be explained by the change in transition scenario and the associated change in length scales. In a previous study, the integral length scales corresponding to a smooth transition case were found to be smaller (i.e., approximately $4D$ in the transition region) and continuously present [14]. This is in contrast to a sharp, intermittent transition, where turbulent patches span about $20D$ – $30D$ [15,18].

All data are shown in the regime map (ϕ vs d/D) in Fig. 2, where each marker represents 1 of 51 complete transition curves (which consist of 11–39 measurements of f vs Re_s). The transition curves with a monotonically decreasing friction factor for increasing Re_s (i.e., $\partial f/\partial Re_s < 0$ for all values of Re) are indicated with squares. The transition curves with a local minimum are represented by triangles. Here the derivative is locally positive in the transition region. The color of the markers indicates $Re_{s,c}$, determined using a threshold of $70/Re$ [9]. This threshold was determined to be a sound balance between robustness to measurement noise and accuracy. Figure 2 confirms the dependence of $Re_{s,c}$ on d/D and ϕ : an increase in either parameter promotes transition. The dashed curve represents a constant Bagnold number [19], which was previously used to classify suspension behavior [13]. It is defined as the ratio of the inertial to viscous stress: $N = d^2 \dot{\gamma} \lambda^{1/2} / \nu$, with $\dot{\gamma}$ being the shear rate and λ being the linear concentration, $1/[(0.74/\phi)^{1/3} - 1]$. The best discrimination between transition mechanisms is found for $N = 7.2$ (based on a bulk shear rate for $Re_{c,0} = 2000$). It is evident that this is still not satisfactory. Alternative values of N will always satisfy only the transition behavior at one d/D . We thus confirm the observation by Lashgari *et al.* [13] that the Bagnold number by itself is not sufficient to predict transition behavior. All experiments shown in Fig. 2 are well below $N = 40$, which suggests that all cases are in the viscous-dominated regime according to Bagnold’s theory. Another model, based on particle agitation versus laminar

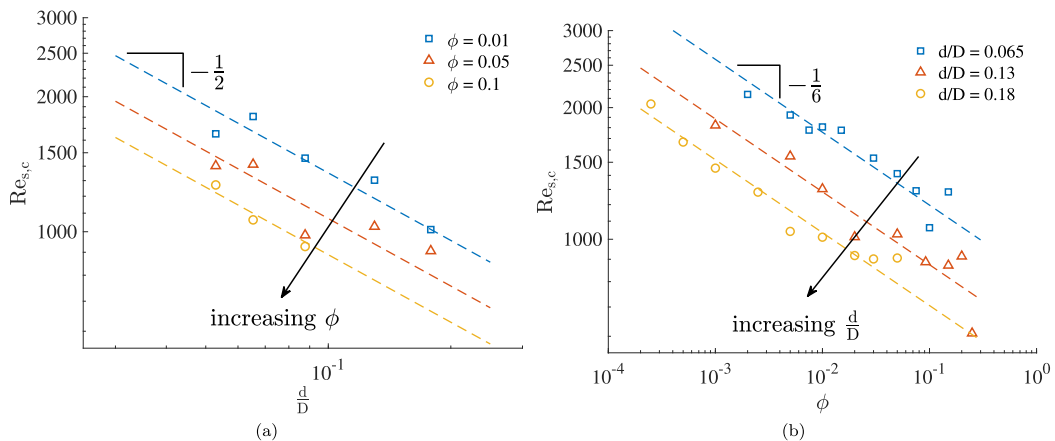


FIG. 3. (a) $Re_{s,c}$ as a function of d/D for three representative volume fractions and (b) $Re_{s,c}$ as function of ϕ for three representative diameter ratios. The dashed curves are based on a regression analysis, where the slope is rounded to the nearest common fraction.

dissipation, was proposed by Leskovec *et al.* [11]. According to their model the threshold between the two mechanisms is predicted by $\phi^2(d/D)^2Re$ and is indicated by the dash-dotted curve. However, this model is based on a limited range of experimental data, resulting in a less accurate prediction for the transition mechanism at higher d/D . The solid curve, indicated by $\epsilon = \text{const}$, is based on our proposed model (introduced below) to distinguish between intermediate and particle-induced transitions.

Previously, it was shown that the velocity fluctuations caused by the finite-sized particles scale with d/D . Based on this, it is expected that $Re_{s,c}$ is dependent on d/D and ϕ [14]. The latter has been shown to be a relevant scaling parameter before [8–10]. The exact respective contributions of d/D and ϕ to $Re_{s,c}$ are studied based on the data shown in Fig. 2. The effects of d/D (for $\phi = 0.01$, 0.05, and 0.1) and ϕ (for $d/D = 0.065$, 0.13, and 0.18) are shown in Figs. 3(a) and 3(b), respectively. In both plots a selection of three representative cases is shown. From both plots it follows that $Re_{s,c}$ depends on d/D and ϕ with exponents of $-\frac{1}{2}$ and $-\frac{1}{6}$, respectively. The exponents are determined using a regression analysis, where the found exponents are rounded to the nearest common fraction. The dashed curves shown are based on this fraction and the corresponding amplitude, resulting from the regression analysis. While both exponents are obtained separately in this approach, we also confirmed that a regression of both exponents simultaneously, $(d/D)^\alpha \phi^\beta$, gave similar results. Note that the square of the linear concentration in Bagnold's scaling also results in an exponent of $\frac{1}{6}$ for the concentration in the dilute limit.

Based on this, the onset of turbulence is modeled as $Re_{s,c}(\frac{d}{D})^{\frac{1}{2}}\phi^{\frac{1}{6}} = c$. Note that the dimensionless group, $(\frac{d}{D})^{\frac{1}{2}}\phi^{\frac{1}{6}}$, can also be interpreted as a perturbation amplitude ϵ resulting from the suspended particles. This is analogous to finite perturbation amplitudes being used in single-phase transition experiments [4,20,21]. Therefore, we decided to introduce the following perturbation amplitude:

$$\epsilon = \left(\frac{d}{D}\right)^{\frac{1}{2}}\phi^{\frac{1}{6}}. \quad (2)$$

This perturbation amplitude can also be rewritten to be proportional to $N_p^{\frac{1}{6}}\frac{d}{D}$, where N_p is the number of particles per unit volume (i.e., D^3). We choose the former representation to separate the parameters, as N_p is a function of both d/D and ϕ . The physical interpretation of ϵ is that the

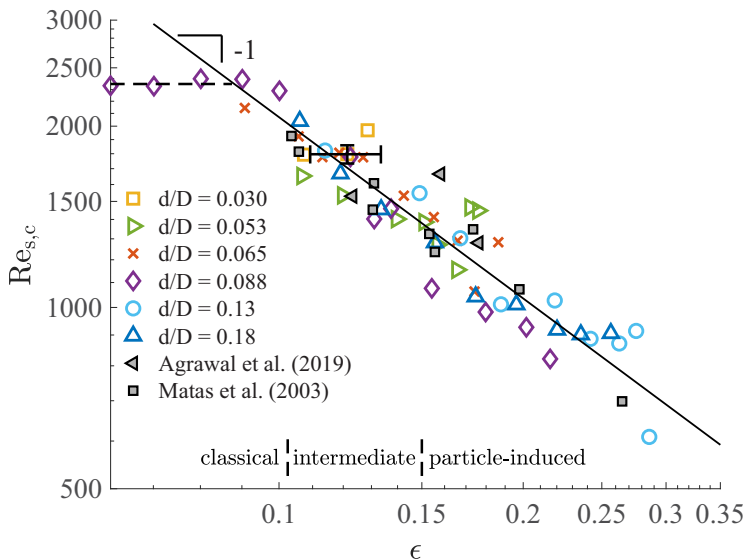


FIG. 4. Critical suspension Reynolds number $Re_{s,c}$ as a function of particle perturbation amplitude ϵ for all experiments. All $Re_{s,c}$ collapse on one single curve with a slope of -1 . The marker on the ordinate axis represents the critical Reynolds number for a single-phase flow $Re_{c,0}$.

perturbation amplitude increases with the number of particles per unit volume and for increasing d/D .

In Fig. 4, all critical Reynolds numbers (i.e., the colors from Fig. 2) are shown as a function of ϵ . As expected, for this scaling all $Re_{s,c}$ now collapse on one single curve given by $Re_{s,c} = 207 \epsilon^{-1}$. The general interpretation of the exponent in the case of single-phase flows is that there is a balance between inertial and viscous forces [21]. For the particle-laden cases the exponents for d/D and ϕ are now responsible for this balance. The prefactor, also resulting from regression, is likely specific for the current configuration: the flow of a suspension of neutrally buoyant, spherical particles through a pipe. The relatively large horizontal error bar, shown for only one experiment, is based on a conservative error propagation and predominantly originates from the polydispersity in particle diameter (common for experimental studies). This scaling is also validated using data from the literature [8,10]. These $Re_{s,c}$ are indicated in the legend. For $Re_{s,c}$ reproduced from Matas *et al.* [8], three $Re_{s,c}$ for three different d/D (i.e., 0.056, 0.063, and 0.1) are shown, spanning a significant range of the scaling. Note that $Re_{s,c}$ beyond the local minimum (see Fig. 3 in Matas *et al.* [8]) are excluded from this analysis as these $Re_{s,c}$ are biased due to their measurement method, as discussed by Hogendoorn and Poelma [9]. Data for $Re_{s,c}$ taken from Agrawal *et al.* [10] also support our scaling.

For small ϵ (i.e., low ϕ and/or d/D), particles will not affect $Re_{s,c}$. In this regime, the amplitude of the particle perturbations is negligible with respect to the perturbation amplitude of the disturbance mechanism. Therefore, the transition behavior will be described by the dashed line in Fig. 4, indicating a fixed transition corresponding to the perturbation amplitude of the used perturbation mechanisms ($Re_{c,0} = 2350$ for this particular experiment). The presence of this plateau is confirmed for experiments with a particle size ratio of $d/D = 0.088$ (see also $Re_{s,c}$ for values of $\epsilon \rightarrow 0$ in Fig. 3 in Matas *et al.* [8]). The marker on the ordinate axis represents the corresponding critical Reynolds number for this single-phase case ($Re_{c,0}$), i.e., $\epsilon \rightarrow 0$.

Using the scaling law, the conditions where the perturbations of the particles are sufficiently damped by viscous effects can be identified, so that transition is not triggered by the particles. For combinations of ϵ and Re_s above the solid line in Fig. 4, the friction factor will deviate 10% or more

from Hagen-Poiseuille’s law. Conversely, for combinations below this line, the friction factor can safely be assumed to be $64/\text{Re}_s$.

The scaling shown in Fig. 4 covers a very wide range of situations, including most engineering applications. As an indication, a 45% volume fraction of particles with a size of 1/10 of the pipe diameter is characterized by $\epsilon = 0.28$. Larger values can be reached by increasing d/D to unity (leading to a theoretical limit of $\epsilon = 0.93$). However, a different scaling is then expected, as these extreme cases would represent stacked particles with a diameter close to the pipe diameter. Obviously, this is no longer a “flowing suspension.”

In the literature, generally, three different regimes are distinguished to describe the underlying dynamics: classical, intermediate, and particle-induced transition behaviors [9,10,14]. Using the perturbation amplitude [Eq. (2)], we can quantitatively distinguish between these different regimes; they are indicated in the bottom of Fig. 4. The border between classical and intermediate transitions can be defined where Re_c is found to deviate from a typical transition Reynolds number for single-phase flow, $\text{Re}_{c,0} = 2000$. The corresponding critical perturbation amplitude is found to be $\epsilon = 0.103$. The change between intermediate and particle-induced transition behaviors is indicated by the solid curve in Fig. 2, corresponding to $\epsilon = 0.15$. This value is determined by minimizing the error between the number of squares and triangles above and below the curve, respectively. Given the limited number of data near the prediction curve, this critical value for ϵ is bounded by 0.135 and 0.17. For simplicity we report a value in the center of this range. Note that there is a smooth transition between classical and particle-induced transition behaviors for increasing ϵ . The intermittent nature of classical transition is gradually replaced by continuous, particle-induced fluctuations; see also the detailed characterization of one single case by Hogendoorn *et al.* [14].

Our motivation to interpret ϵ as a perturbation amplitude follows from similar approaches in single-phase flow experiments [20,21]. Note that for suspension flows the particle-induced perturbations are continuously present along the length of the pipe. This is in contrast to single-phase perturbation experiments, where the perturbation is temporally and spatially bounded. For injection-based disturbances the perturbation amplitude is typically defined as the ratio of the injection volume flux with respect to the volume flux in the pipe. Similarly, for an orifice-type perturbation the orifice diameter can be expressed as a disturbance amplitude. The amplitude required to trigger a transition in single-phase flows scales with Re^γ , where the exponent varies between -1 and -1.5 , depending on the type of perturbation [4,21,22]. This scaling is generally based on experiments for $\text{Re} > 2000$, while for particle-laden flows the range *below* $\text{Re}_s = 2000$ is especially important.

Further measurements with small d/D and/or low ϕ (i.e., low ϵ) in the absence of a perturbation mechanism should reveal the flow stability response for $\text{Re}_{s,c} > 2000$. This will also shed light on the universality of the various perturbation parameters. On the edges of the investigated parameter space (Fig. 2) various effects will come into play [23]. For instance, the effect of the spatial distribution of particles on the transition in the (semi)dilute regime is still an open question. For $d/D \rightarrow 0$, our model predicts that particles will not affect the transition, but this needs to be confirmed. Additionally, measurements for higher volume fractions need to be performed to establish whether our scaling law will hold in the inertial shear-thickening regime [13].

In summary, based on a large set of experimental data, we uncovered a scaling law relating the amplitude of the particle-induced perturbations to the critical suspension Reynolds number. The particle-induced perturbation amplitude is a simple function of the particle-to-pipe diameter ratio and the volume fraction: $\epsilon = (d/D)^{1/2}\phi^{1/6}$. The onset of turbulence in neutrally buoyant suspensions was found to scale as $\text{Re}_{s,c} \sim \epsilon^{-1}$. Data from the literature also support the validity of this scaling. Furthermore, ϵ allows a prediction of the transition scenario. For a variety of applications it will predict whether the transition will be classical, intermediate, or particle induced.

Underlying data are deposited in 4TU.ResearchData [24].

We thank V. Krishnan for assisting in our experimental campaign. We would like to thank S. van Baal (Synthos EPS) for kindly providing particles for this research. This work is funded by ERC Consolidator Grant No. 725183 “OpaqueFlows.”

- [1] O. Reynolds, An experimental investigation of the circumstances which determine whether the motion of water shall be direct or sinuous, and of the law of resistance in parallel channels, *Philos. Trans. R. Soc. London* **174**, 935 (1883).
- [2] P. G. Drazin and W. H. Reid, *Hydrodynamic Stability* (Cambridge University Press, Cambridge, 2004).
- [3] R. Kerswell, Recent progress in understanding the transition to turbulence in a pipe, *Nonlinearity* **18**, R17 (2005).
- [4] B. Hof, A. Juel, and T. Mullin, Scaling of the Turbulence Transition Threshold in a Pipe, *Phys. Rev. Lett.* **91**, 244502 (2003).
- [5] D. J. Kuik, C. Poelma, and J. Westerweel, Quantitative measurement of the lifetime of localized turbulence in pipe flow, *J. Fluid Mech.* **645**, 529 (2010).
- [6] B. Hof, J. Westerweel, T. M. Schneider, and B. Eckhardt, Finite lifetime of turbulence in shear flows, *Nature (London)* **443**, 59 (2006).
- [7] K. Avila, D. Moxey, A. de Lozar, M. Avila, D. Barkley, and B. Hof, The onset of turbulence in pipe flow, *Science* **333**, 192 (2011).
- [8] J.-P. Matas, J. F. Morris, and E. Guazzelli, Transition to Turbulence in Particulate Pipe Flow, *Phys. Rev. Lett.* **90**, 014501 (2003).
- [9] W. Hogendoorn and C. Poelma, Particle-Laden Pipe Flows at High Volume Fractions Show Transition without Puffs, *Phys. Rev. Lett.* **121**, 194501 (2018).
- [10] N. Agrawal, G. H. Choueiri, and B. Hof, Transition to Turbulence in Particle Laden Flows, *Phys. Rev. Lett.* **122**, 114502 (2019).
- [11] M. Leskovec, F. Lundell, and F. Innings, Pipe flow with large particles and their impact on the transition to turbulence, *Phys. Rev. Fluids* **5**, 112301(R) (2020).
- [12] I. M. Krieger, Rheology of monodisperse latices, *Adv. Colloid Interface Sci.* **3**, 111 (1972).
- [13] I. Lashgari, F. Picano, W.-P. Breugem, and L. Brandt, Laminar, Turbulent, and Inertial Shear-Thickening Regimes in Channel Flow of Neutrally Buoyant Particle Suspensions, *Phys. Rev. Lett.* **113**, 254502 (2014).
- [14] W. Hogendoorn, B. Chandra, and C. Poelma, Suspension dynamics in transitional pipe flow, *Phys. Rev. Fluids* **6**, 064301 (2021).
- [15] I. J. Wygnanski and F. Champagne, On transition in a pipe. Part 1. The origin of puffs and slugs and the flow in a turbulent slug, *J. Fluid Mech.* **59**, 281 (1973).
- [16] A. A. Draad, G. Kuiken, and F. Nieuwstadt, Laminar–turbulent transition in pipe flow for Newtonian and non-Newtonian fluids, *J. Fluid Mech.* **377**, 267 (1998).
- [17] J. J. Stickel and R. L. Powell, Fluid mechanics and rheology of dense suspensions, *Annu. Rev. Fluid Mech.* **37**, 129 (2005).
- [18] B. Eckhardt, T. M. Schneider, B. Hof, and J. Westerweel, Turbulence transition in pipe flow, *Annu. Rev. Fluid Mech.* **39**, 447 (2007).
- [19] R. A. Bagnold, Experiments on a gravity-free dispersion of large solid spheres in a Newtonian fluid under shear, *Proc. R. Soc. London, Ser. A* **225**, 49 (1954).
- [20] F. Waleffe, On a self-sustaining process in shear flows, *Phys. Fluids* **9**, 883 (1997).
- [21] T. Mullin, Experimental studies of transition to turbulence in a pipe, *Annu. Rev. Fluid Mech.* **43**, 1 (2011).
- [22] J. Peixinho and T. Mullin, Finite-amplitude thresholds for transition in pipe flow, *J. Fluid Mech.* **582**, 169 (2007).
- [23] J. F. Morris, Toward a fluid mechanics of suspensions, *Phys. Rev. Fluids* **5**, 110519 (2020).
- [24] <https://doi.org/10.4121/16586954>.